Journal of Alloys and Compounds 611 (2014) 335–340

Contents lists available at ScienceDirect

Journal of Alloys and Compounds

journal homepage: www.elsevier.com/locate/jalcom

Controllable one-pot synthesis of various one-dimensional Bi_2S_3 nanostructures and their enhanced visible-light-driven photocatalytic reduction of Cr(VI)

Enlai Hu [a,1], Xuehui Gao [a,1], Atangana Etogo [a], Yunlong Xie [a], Yijun Zhong [b,*], Yong Hu [a,*]

[a] Key Laboratory of the Ministry of Education for Advanced Catalysis Materials, Institute of Physical Chemistry, Zhejiang Normal University, Jinhua 321004, PR China
[b] College of Chemistry and Life Sciences, Zhejiang Normal University, Jinhua 321004, PR China

ARTICLE INFO

Article history:
Received 18 February 2014
Received in revised form 11 May 2014
Accepted 12 May 2014
Available online 2 June 2014

Keywords:
1D Bi_2S_3 nanostructures
One-pot synthesis
Photoactivity
Cr(VI) reduction

ABSTRACT

One-dimensional (1D) Bi_2S_3 nanostructures with various morphologies, including nanowires, nanorods, and nanotubes, have been successfully synthesized through a facile ethanol-assisted one-pot reaction. It is found that the size, morphology and structure of the products can be conveniently varied or controlled by simply adjusting the volume ratio of ethanol and water in the reaction system. Further experimental results indicate that sulfur source also plays the other crucial role in determining the product morphology. The synthetic strategy developed in this work is highly efficient in producing 1D Bi_2S_3 nanostructures with high quality and large quantity. Photocatalysis experiments show the as-prepared 1D Bi_2S_3 nanostructures possess significantly enhanced photocatalytic reduction of Cr(VI) when exposed to visible light irradiation. Especially, Bi_2S_3 nanowires exhibit the highest photocatalytic activity and can be used repeatedly after washed with dilute HCl.

1. Introduction

One-dimensional (1D) nanostructures have attracted tremendous research attention owing to their unique optical, electrical, catalytic and magnetic properties, etc. [1–3]. Especially, the fabrication of 1D semiconductor nanostructures with controllable shape and size is extremely important from the viewpoints of both fundamental research and technical applications [4–9]. Bismuth sulfide (Bi_2S_3), an important V–VI semiconductor material with a direct band gap of 1.3 eV [10–13], has aroused extensive research interest for various potential applications in photovoltaics [14], X-ray computed tomography imaging (CT) [15], lithium ion battery [16], hydrogen sensors [17,18], photocatalysis [19,20], and so on. Benefitting from high aspect ratio, enhanced light scattering and absorption, rapid transport of free electron along the long axis and efficient electron–hole utilization, 1D nanostructures exhibit significantly enhanced catalytic efficiency [21,22]. Thus, the photocatalytic activity of 1D Bi_2S_3 nanostructures is worth investigating especially in terms of environmental treatment.

To date, 1D Bi_2S_3 nanostructures with various morphologies, including nanotubes (NTs) [23], nanorods (NRs) [24,25], nanowires (NWs) [26], nanoribbons [27], have been prepared by different methods, among which solution-phase approaches have been extensively adopted due to the advantages of relatively low-cost and good scalability. However, the seeking of a facile and scalable preparation method with high quality and yield has never been a trivial task. The formation of 1D nanostructures in solution is typically realized by facilitating the crystal growth along a particular direction with the assistance of capping agents [28,29].

In this work, we have developed a facile ethanol-assisted one-pot reaction route to synthesize 1D Bi_2S_3 nanostructures with various morphologies, including NWs, NRs, and NTs. In the present strategy, we found that the size, morphology and structure of the products can be conveniently varied or controlled by the adjustment of the volume ratio of ethanol and water in the reaction system. Further experimental results indicate that sulfur source also plays a crucial role in determining the morphologies of Bi_2S_3 products. It should be pointed out that the one-pot reaction method developed in this work is highly efficient in producing 1D Bi_2S_3 nanostructures in large-scale. For example, about 0.0801 g of Bi_2S_3 NWs (using 0.1 g of $BiCl_3$ as reagent) can be obtained in 40 mL of ethanol, with a yield up to 98%. Further investigation also shows the as-prepared 1D Bi_2S_3 nanostructures possess significantly enhanced photocatalytic reduction of Cr(VI) under visible-light illumination. Especially, Bi_2S_3 NWs exhibit the

* Corresponding authors. Tel.: +86 579 82282234; fax: +86 579 82282595.
E-mail addresses: yjzhong@zjnu.cn (Y. Zhong), yonghu@zjnu.edu.cn (Y. Hu).
[1] These authors contributed equally to this work.

http://dx.doi.org/10.1016/j.jallcom.2014.05.075
0925-8388/

best photocatalytic activity due to higher aspect ratio and can be used repeatedly after washed with dilute HCl.

2. Experimental details

All reagents are of analytical grade, purchased from the Shanghai Chemical Reagent Factory, and used as received without further purification.

2.1. Synthesis of Bi_2S_3 NWs

In a typical procedure, 0.1 g of $BiCl_3$ and 0.5 g of polyvinylpyrrolidone (PVP; MW ~ 58 K) were dissolved in 25 mL of ethanol with the assistance of ultrasonication for 20 min to form a clear mixture, which was marked as solution A. 0.038 g of thioacetamide (TAA) was dissolved in the 15 mL of ethanol with the assistance of ultrasonication for 10 min, and marked as solution B. Then, the solution B was added dropwise to solution A under vigorous stirring. The resulting mixture was then transferred into a 50 mL of Teflon-lined stainless-steel autoclave, and then kept at 180 °C for 6 h in an electric oven. Finally, after cooled to room temperature, the Bi_2S_3 NW products were collected by centrifugation, washed with ethanol and distilled water for three times, and then dried at 80 °C for 4 h.

2.2. Synthesis of Bi_2S_3 NRs and NTs

1D Bi_2S_3 NRs were prepared with the same procedures as Bi_2S_3 NWs, except that the distilled water was used to dissolve TAA in preparing solution B. 1D Bi_2S_3 NTs were obtained with the same experimental conditions as Bi_2S_3 NRs except that $Na_2S{\cdot}9H_2O$ (0.126 g) was selected as sulfur source. Other Bi_2S_3 nanostructures were obtained by simply adjusting the volume ratio of ethanol and water in the reaction system. The detailed conditions for the preparation of the products with various morphologies are listed in Table 1.

2.3. Characterization

Powder X-ray diffraction (XRD) measurements of the samples were performed with a Philips PW3040/60 X-ray diffractometer using Cu Kα radiation at a scanning rate of 0.06 deg s^{-1}. Scanning electron microscopy (SEM) was performed with a Hitachi S-4800 scanning electron micro-analyzer with an accelerating voltage of 15 kV. Transmission electron microscopy (TEM) was conducted using a JEM-2100F field emission TEM. Samples for TEM measurements were prepared by dispersing the products in ethanol and placing several drops of the suspension on holey carbon net supported on copper grids. UV–vis diffuse reflectance spectra (UV–vis DRS) of the as-prepared samples were recorded over the range of 200–800 nm with the absorption mode using a Thermo Nicolet Evolution 500 UV–vis spectrophotometer equipped with an integrating sphere attachment. The photoluminescence (PL) spectra were recorded on an Edinburgh FLSP920 fluorescence spectrometer with an excitation wavelength of 462 nm and the absorption spectra were measured using a PerkinElmer Lambda 900 UV–vis spectrophotometer at room temperature.

2.4. Photocatalytic reduction of Cr(VI)

The photocatalytic activities of the as-prepared Bi_2S_3 NWs, NRs and NTs were evaluated by photocatalytic reduction of Cr(VI) under visible-light irradiation of a 500 W Xe lamp (CEL-HXF300) with a 420 nm cut-off filter. The reaction cell was placed in a sealed black box with a window on the top, and the cut-off filter was used to select visible-light irradiation. In a typical procedure, 5 mg of as-prepared Bi_2S_3 NWs, NRs or NTs as photocatalysts were added into 20 mL of Cr(VI) solutions (20 mg/L), based on Cr in a dilute $K_2Cr_2O_7$ solution. After the photocatalyst was dispersed in the solution with an ultrasonic bath for 5 min, the solution was stirred for 2 h in the dark to reach adsorption equilibrium before exposed to visible-light irradiation. The photocatalysts were removed by centrifugation at given time intervals, and the Cr(VI) reduction was determined at 540 nm by the diphenylcarbazide (DPC) method using the UV–vis spectroscopy [30,31].

Table 1
Summary of experimental conditions and the morphological properties of the products.

No.	$BiCl_3$ (g)	Sulfur source (mg)	Solvent		Yield (%)	Bi_2S_3 product
			Ethanol	Water		
S1	0.1	TAA (35)	40	0	98.2	NWs
S2	0.1	TAA (35)	25	15	90.9	NRs
S3	0.1	TAA (35)	20	20		NRs
S4	0.1	TAA (35)	15	25		Short NRs
S5	0.1	TAA (35)	0	40		Nanosheets
S6	0.1	Na_2S (170)	35	5		Nanoparticles
S7	0.1	Na_2S (170)	25	15	86.9	NTs
S8	0.1	Na_2S (170)	20	20		NTs
S9	0.1	Na_2S (170)	15	25		NTs

3. Results and discussion

The crystallographic structure and phase purity of the as-obtained ultralong Bi_2S_3 NWs (sample S1) were first examined by XRD analysis, as shown in Fig. 1. All the diffraction peaks can be well indexed to the orthorhombic phase of Bi_2S_3 (JCPDS card No. 17-0320, a = 11.14 Å, b = 11.30 Å, c = 3.98 Å). No peaks due to impurity or other phases are detected, implying that the final products are of pure phase. Additionally, the XRD patterns of the as-prepared Bi_2S_3 NRs (sample S2) and NTs (sample S7) all show a similar profile to that of Bi_2S_3 NWs. The morphology and structure of the Bi_2S_3 NWs (S1) were studied by SEM and TEM images. Fig. 2a and b shows the SEM images of a panoramic view of the as-prepared NWs (S1) obtained by using ethanol as solvent and TAA as sulfur source, which reveal that the samples are entirely composed of uniform ultralong Bi_2S_3 NWs, 10 nm in diameter and dozens of micrometers in length, without any impurity particles or aggregates. The morphology and structure of these Bi_2S_3 NWs were further elucidated by TEM and high-resolution TEM (HRTEM) images. Fig. 2c is a TEM image of Bi_2S_3 NWs and the inset is an individual Bi_2S_3 NW, which are in good agreement with the SEM observation. A representative HRTEM image (Fig. 2d) reveals two interplanar distances of 0.37 and 0.55 nm, which match well with that of (101) and (200) lattice of orthorhombic phase Bi_2S_3, respectively [32].

To investigate the effect of the relative volume of ethanol and water in the mixed solvent on the product morphology (the total ethanol/water volume is fixed at 40 mL), a series of experiments were carried out with varied the volume of ethanol added in the reaction system while keeping other conditions unchanged. Fig. 3a–c displays the structure of the samples synthesized with a decreasing of the volume of ethanol from 25 mL to 15 mL in the reaction solution. From these images, with the decrease of the amount of ethanol, the as-obtained products become shorter and wider, indicating a gradual conversion of NWs to NRs. However, when the ethanol was absent, only Bi_2S_3 nanosheets were formed in water (Fig. 3d). Based on these observations, it might be apparent that the volume ratio of ethanol and water plays a critical role in the formation of 1D Bi_2S_3 NWs and NRs in the reaction system. The use of TAA as the sulfur source to control the morphology of 1D Bi_2S_3 in the solution phase has been previously investigated [33,34]. It was suggested that Bi_2S_3 material has a lamellar structure composed of Bi_2S_3 bands elongating along the c-axis and kept together through van der Waals interactions, which

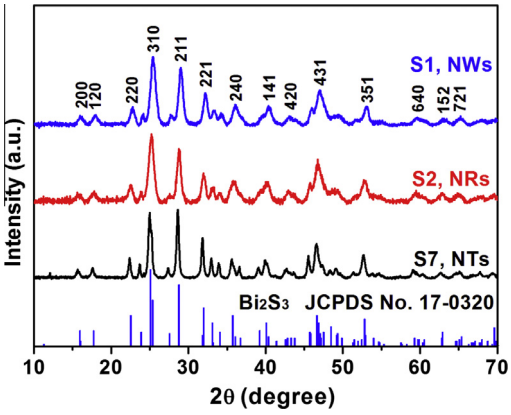

Fig. 1. XRD patterns of the as-prepared Bi_2S_3 NWs (S1), NRs (S2) and NTs (S7).

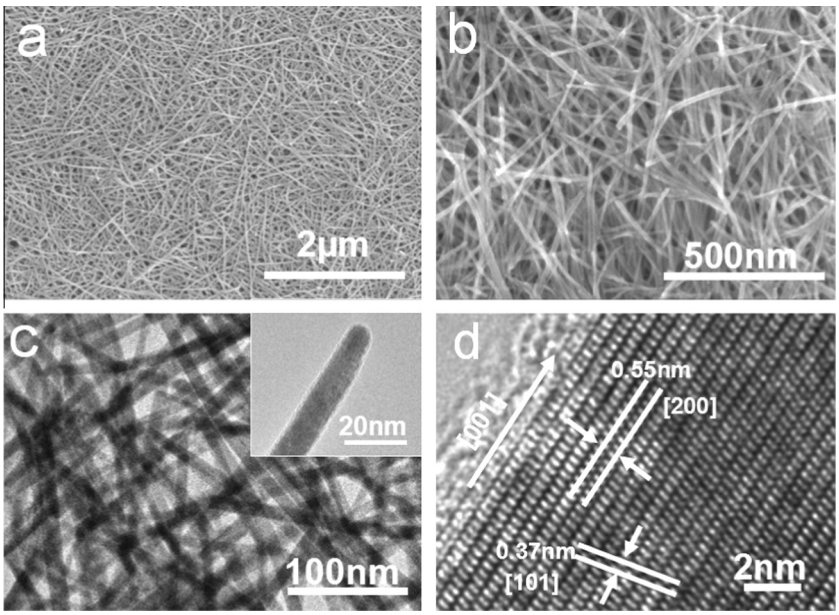

Fig. 2. (a, b) SEM images and (c) TEM image and (d) HRTEM image of the as-prepared Bi_2S_3 NWs obtained in ethanol.

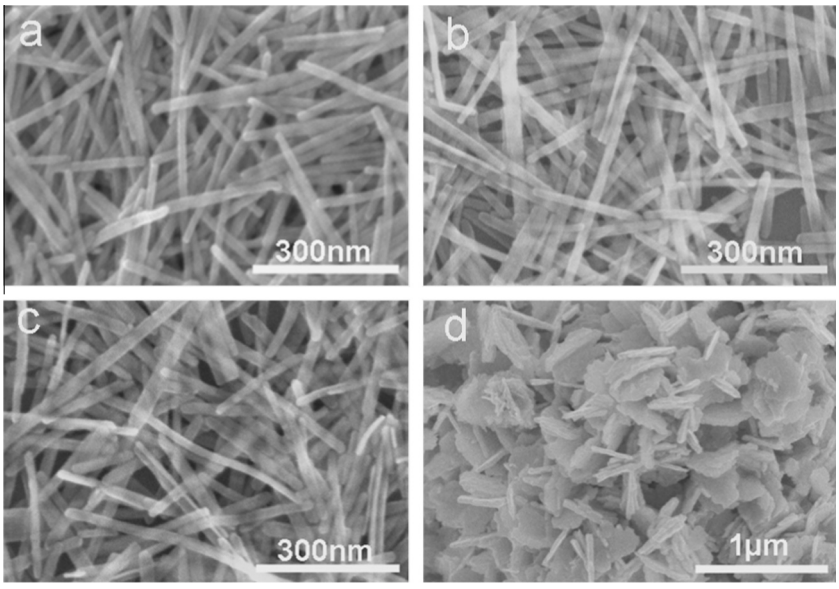

Fig. 3. SEM images of the as-prepared Bi_2S_3 nanostructures using TAA as sulfur source obtained with different amount of water: (a)15 mL, (b) 20 mL, (c) 25 mL, and (d) 40 mL.

resulted in a strong tendency toward 1D growth along the [001] direction [35]. On the other hand, it is well known that solubility is one of the most important factors affecting single crystal growth in a solution [36]. In our experiment, the formation of ultralong NWs can readily occur in a metastable, supersaturated solution by controlling the volume of ethanol and water. Due to lower solubility of Bi^{3+} ions salts in ethanol, a metastable, supersaturated solution could be obtained, and the growth of ultralong Bi_2S_3 NWs presumably took place, similar to the transformation of polycrystalline selenium powder into single-crystal NWs [37]. Therefore, with the increasing volume of water, the NWs were gradually converted into NRs. When the pure water is used as solvent, there is a dynamic equilibrium among Bi_2S_3 solid particles (or nuclei) and Bi^{3+} and S^{2-} ions in the hydrothermal process. Bi^{3+} and S^{2-} ions tend to dissolve away from the small particles into the solution and precipitate onto the surfaces of large particles at the same time. Due to the special layered structure and weak bonds of Bi_2S_3, the nucleation can be confirmed by the appearance of tiny thin crystals in the solution [38]. In the hydrothermal treatment, the rate of crystal growth is greater than that of crystal nucleation, leading to the growth of Bi_2S_3 nanosheets [39].

When Na_2S was used instead of TAA as sulfur source, neither NWs nor NRs can be obtained in the final products. The morphologies of the as-prepared samples S6–S9 obtained with the different volumes of ethanol and water in the reactive system are shown in Fig. 4. Fig. 4a shows a SEM image of the products obtained with the use of 5 mL of water, it can be seen that only some Bi_2S_3 conglomerations are formed. When the volume of water increases to 15 mL, the products (sample S7) exhibit a tubular-like morphology with a lateral diameter of 200–300 nm and a length of 1 μm (Fig. 4b).

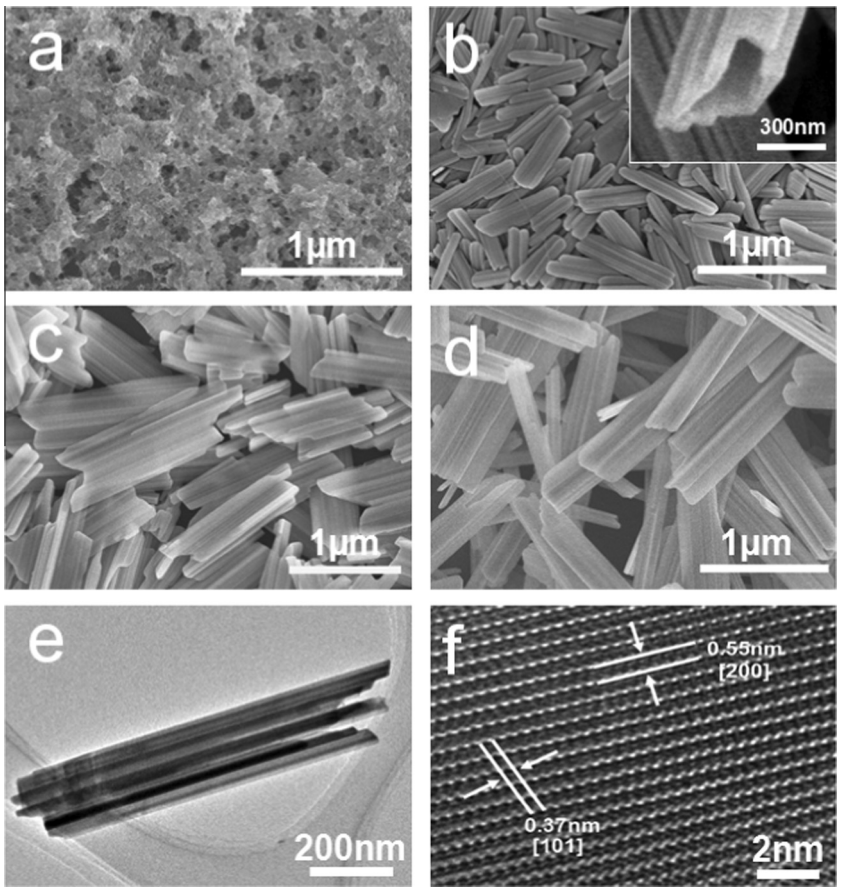

Fig. 4. SEM images of the as-prepared Bi_2S_3 nanostructures using Na_2S as sulfur source obtained with different amount of water: (a) 5 mL, (b) 15 mL, (c) 20 mL, and (d) 25 mL, (e) TEM image and (f) HRTEM image the as-prepared Bi_2S_3 NTs (S7).

From the inset of SEM image in Fig. 4b, the tip structure of a single NT display the obvious hollow characteristic in the end of the NT. Fig. 4c–d shows that the as-prepared Bi_2S_3 NTs become longer and wider with the increase of the volumes of water in the reaction system. The NTs may be obtained by self-rolling of nanosheets under an appropriate solvothermal synthesis condition [40]. This result indicates that the nature of sulfur sources also plays an important role in the morphology control of Bi_2S_3 besides the volume ratio between ethanol and water in the present synthetic strategy. The tubular structure of the Bi_2S_3 NTs (S7) was further elucidated by TEM and HRTEM images, as shown in Fig. 4e and f. This result is in good agreement with the SEM observation.

To investigate the optical properties of the as-prepared 1D Bi_2S_3 nanostructures and their potential applications as photonic materials, UV–vis diffuse reflectance spectra of the different 1D Bi_2S_3 nanostructures (NWs, NRs, and NTs) were carried out, as shown in Fig. S1a (in the supporting information). All of the spectra exhibit the strong adsorption in the UV–visible region and had a broad peak between 650 and 800 nm [41]. The optical bandgap (E_g) of the semiconductor material can be calculated from the equation of $(\alpha h\nu)^n = A(h\nu - E_g)$, where α, ν, E_g, and A are the absorption coefficient, light frequency, band gap energy, and a constant, respectively. Among them, n depends on the characteristics of the transition in a semiconductor (i.e., $n = 2$ for direct transition or $n = 1$ for indirect transition). Herein, n is 2 as the material is a direct-gap semiconductor [42,43]. From the plot of $(\alpha h\nu)^2$ vs. $(h\nu)$ (Fig. S1b), the E_g of Bi_2S_3 NWs is calculated to be 1.3 eV. In addition, the estimated band gap energies of the other samples are about 1.5 and 1.75 eV for Bi_2S_3 NRs (S2) and NTs (S7), respectively. The absorption of the Bi_2S_3 NRs and NTs show a blue shift compared with the band gap of 1.3 eV for the Bi_2S_3 NWs, which could be associated with the morphology, size and structure. The PL spectra of the as-prepared 1D Bi_2S_3 nanostructures were further investigated to understand the separation efficiency of the photogenerated carriers [44], as shown in Fig. S2 (in the supporting information). The higher the PL intensity will lead to the bigger probability of charge carriers recombination. The strong peak at 577 nm may be ascribed to a high level transition in Bi_2S_3 semiconductor crystallites [45]. The intensity for the Bi_2S_3 NWs (S1) is much weaker than that for the other samples, indicting the enhanced separation efficiency of the electron–hole pairs.

Recent studies have suggested that 1D nanostructures exhibit significantly enhanced catalytic efficiency due to high surface-to-volume ratio, enhanced light scattering and absorption, rapid transport of free electron along the long axis and efficient electron–hole utilization [46–50]. As a proof-of-concept demonstration of the functional properties of the as-prepared 1D Bi_2S_3 nanostructures, the photocatalytic activities were evaluated by photocatalytic reduction of Cr(VI) under visible-light irradiation in the present work. Fig. 5a presents the visible-light photocatalytic reduction of Cr(VI) in the presence of different photocatalysts, where C stands for the concentration of Cr(VI) after light irradiation for a certain period, and Co is the initial concentration of the Cr(VI). In the absence of the catalysts, there is no obvious change in the Cr(VI) concentration after visible-light irradiation. When the 1D Bi_2S_3 samples are present, remarkable reduction of Cr(VI) is observed. After irradiation for 60 min, nearly 85.1% of Cr(VI) is photocatalytically reduced by the Bi_2S_3 NWs, whereas the other

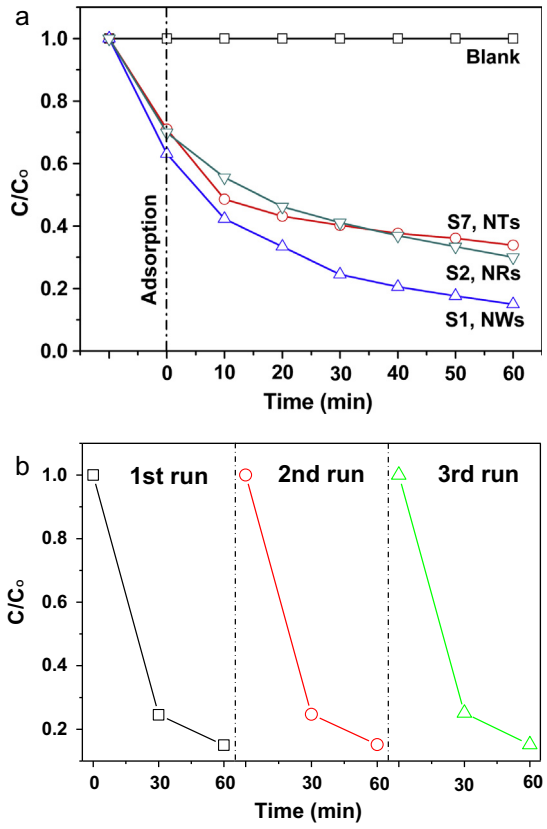

Fig. 5. (a) The photocatalytic reduction of Cr(VI) in the absence (the blank test) and in the presence of different photocatalysts under visible-light illumination. (b) 3 Cycles of the photocatalytic reduction of Cr(VI) using Bi_2S_3 NWs (sample S1) as the photocatalyst under visible-light irradiation for 60 min.

samples such as Bi_2S_3 NRs and NTs exhibit lower activities with removal rates of about 69.9% and 66.1%, respectively. This result indicates the higher aspect ratio is beneficial for inhibition of photogenerated electrons and holes, and therefore the as-prepared ultralong Bi_2S_3 NWs (sample S1) exhibits the highest photocatalytic activity among the three samples. Additionally, the surface area of the as-prepared Bi_2S_3 NWs, NRs, and NTs was measured by the Brunauer–Emmet–Teller (BET) method using an ASAP2020 sorptometer. The Bi_2S_3 NWs have a specific surface area of about 32.3 $m^2\,g^{-1}$, and it is only about 27.1 or 10.3 $m^2\,g^{-1}$ for the NRs or NTs, respectively. Thus, the enhanced photocatalytic activity might be related to the unique Bi_2S_3 NWs, which gives a large surface area.

The reusability and stability of the 1D ultralong Bi_2S_3 NWs (S1) were also investigated by collecting and reusing the same photocatalyst for 3 cycles (Fig. 5b). After the photocatalytic reduction of Cr(VI), the $Cr(OH)_3$ would be deposited on the surface of Bi_2S_3 NWs, which occupies the photocatalytically active sites, resulting in serious deactivation of the photocatalyst for reusability [51,52]. To overcome this obstacle, the washing treatment with dilute HCl aqueous solution (0.5 M) was used in the present strategy. Fig. 6 displays the SEM image and XRD pattern of the sample S1 photocatalyst after three cycles of photodegradation testing, indicating the intact morphology and stable structure. The results show that there is only an insignificant loss in the photocatalytic activity, which might be partly caused by loss of the photocatalyst during each round of collection and rinsing. In addition, the photocatalytic performances of the as-obtained Bi_2S_3 NWs and several typical photocatalysts for the reduction of Cr(VI) under visible-light illumination reported previously are summarized in Table S1 (in the supporting information).

The effect of pH on the photocatalytic reduction of Cr(VI) using the as-prepared Bi_2S_3 NWs (S1) as photocatalysts was also investigated, as shown in Fig. S3. The various values of pH have an obvious influence on the reduction of Cr(VI), and the photocatalytic reduction would be more efficient at acidic conditions. For example, the reduction efficiency is nearly 99.9% at pH = 3 after visible-light irradiated for 20 min, while only about 75% for pH 10 and 85.1% for pH 7 are reduced after 60 min, respectively. The similar result concerning the beneficial effect of decreasing solution pH on Cr(VI) photocatalytic reduction have been reported elsewhere [53]. To further understand the photocatalytic mechanism, the identification of the main active oxidant (reactive oxygen species) in the photocatalytic reaction process was also carried out. Fig. S4 reveals the photocatalytic activity for the reduction of Cr(VI) by the radical-trapping experiments conducted by the addition of 7 mg of disodium ethylenediaminetetraacetate dehydrate (EDTA-Na_2, hole scavenger) or 2 mL of tert-butyl alcohol (TBA, radical scavenger) [54] using the as-prepared Bi_2S_3 NWs (S1) as photocatalysts, indicating these scavengers have no obvious influence on reduction efficiency. Thus, the photogenerated electrons are the dominant reactive species contributing to reduction of Cr(VI) in this system. Additionally, thermogravimetric analysis (TGA) experiment (Fig. S5) was investigated to understand the thermostability of the as-prepared Bi_2S_3 NWs (S1) in air with heating rate of 10 °C/min. The loss of mass between 400 °C and 680 °C is about 8.01%, which nearly agree with calculated weight loss from molecular formula 9.40%. The thermal event starting near 400 °C and ending neat 450 °C corresponds to an small increase in residual mass, which may be ascribed to the formation of $Bi_2O_2(SO_4)$ [55].

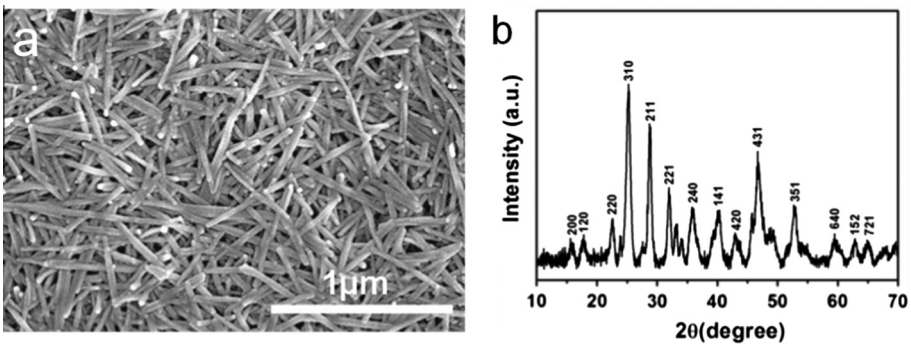

Fig. 6. (a) SEM image and (b) XRD pattern of the Bi_2S_3 NWs (sample S1) after three cycles of photodegradation test.

4. Conclusions

In summary, we have developed a facile ethanol-assisted one-pot reaction route to synthesize 1D Bi_2S_3 nanostructures (NWs, NRs, and NTs) with high productivity and yield. We found that the size, morphology and structure of the products can be conveniently varied or controlled by simply adjusting the volume ratio of ethanol and water in the reaction system. Additionally, further experimental results also indicate that sulfur source also plays another crucial role in determining the morphologies of Bi_2S_3 products. Due to higher aspect ratio, the as-prepared ultralong Bi_2S_3 NWs exhibits the best photocatalytic activity among all the 1D Bi_2S_3 nanostructures, as well as good reusability and stability after washed with dilute HCl. Therefore, the 1D Bi_2S_3 NWs may be applied as a promising photocatalyst for the treatment of wastewater. It is also believed that the synthesis method reported here can be easily extended to the preparation of a wide variety of functional 1D nanostructures for different applications.

Acknowledgement

Financial supports from the Natural Science Foundation of China (21171146), the Zhejiang Provincial Natural Science Foundation of China (LR14B010001), and the Plan Project of Science and Technology in Zhejiang Province (2012C23049) are gratefully acknowledged.

Appendix A. Supplementary material

Supplementary data associated with this article can be found, in the online version, at http://dx.doi.org/10.1016/j.jallcom.2014.05.075.

References

[1] M. Fang, H.Q. Wang, X.L. Tan, B.C. Cheng, L.D. Zhang, Z.D. Xiao, J. Alloys Comp. 457 (2008) 413–416.
[2] G.V. Bazuev, A.P. Tyutyunnik, I.F. Berger, I.V. Nikolaenko, B.G. Golovkin, J. Alloys Comp. 509 (2011) 6158–6162.
[3] Y. Hu, H.H. Qian, Y. Liu, G.H. Du, F.M. Zhang, L.B. Wang, X. Hu, CrystEngComm 13 (2011) 3438–3443.
[4] S. Krishnan, A.S.M.A. Haseeb, M.R. Johan, J. Alloys Comp. 586 (2014) 360–367.
[5] D.M. Cunha, F.L. Souza, J. Alloys Comp. 577 (2013) 158–164.
[6] X.Z. Zeng, X. Zhang, M. Yang, Y.X. Qi, Mater. Lett. 112 (2013) 87–89.
[7] W.J. Chen, L.Y. Zheng, M.L. Wang, Y.W. Chi, G.N. Chen, Anal. Chem. 85 (2013) 9655–9663.
[8] S.H. Park, H.S. Shin, Y.H. Kim, H.M. Park, J.Y. Song, J. Alloys Comp. 580 (2013) 152–156.
[9] P.S. Venkatesh, V. Ramakrishnan, K. Jeganathan, Mater. Res. Bull. 48 (2013) 3811–3816.
[10] H.F. Bao, C.M. Li, X.Q. Cui, Y. Gan, Q.L. Song, J. Guo, Small 4 (2008) 1125–1129.
[11] X. Huang, Y. Yang, X. Dou, Y. Zhu, G. Li, J. Alloys Comp. 461 (2008) 427–431.
[12] M. Salavati-Niasari, D. Ghanbari, F. Davar, J. Alloys Comp. 488 (2009) 442–447.
[13] X.L. Du, F.S. Cai, X.W. Wang, J. Alloys Comp. 587 (2014) 6–9.
[14] G. Konstantatos, L. Levina, J. Tang, E.H. Sargent, Nano Lett. 8 (2008) 4002–4006.
[15] O. Rabin, J.M. Perez, J. Grimm, G. Wojtkiewicz, R. Weissleder, Nat. Mater. 5 (2006) 118–122.
[16] H.Y. Zhou, S.L. Xiong, L.Z. Wei, B.J. Xi, Y.C. Zhu, Y.T. Qian, Cryst. Growth Des. 9 (2009) 3862–3867.
[17] C.F. Guo, S.H. Cao, J.M. Zhang, H.Y. Tang, S.M. Guo, Y. Tian, Q. Liu, J. Am. Chem. Soc. 133 (2011) 8211–8215.
[18] G.J. Xiao, Q.F. Dong, Y.N. Wang, Y.M. Sui, J.J. Ning, Z.Y. Liu, W.J. Tian, B.B. Liu, G.T. Zou, B. Zou, RSC Adv. 2 (2012) 234–240.
[19] T. Wu, X.G. Zhou, H. Zhang, X.H. Zhong, Nano Res. 3 (2010) 379–386.
[20] F.J. Chen, Y.L. Cao, D.Z. Jia, J. Colloid Interface Sci. 404 (2013) 110–116.
[21] Y. Liu, L. Zhou, Y. Hu, C.F. Guo, H.S. Qian, F.M. Zhang, X.W. Lou, J. Mater. Chem. 21 (2011) 18359–18364.
[22] M.J. Zhou, Y. Hu, Y. Liu, W.L. Yang, H.S. Qian, CrystEngComm 14 (2012) 7686–7693.
[23] J.L. Wu, F. Qin, G. Cheng, H. Li, J.H. Zhang, Y.P. Xie, H.J. Yang, Z. Lu, X.L. Yu, R. Chen, J. Alloys Comp. 509 (2011) 2116–2126.
[24] U. Thupakula, J.K. Bal, A. Debangshi, A.H. Khan, A. Dalui, S. Acharya, J. Phys. Chem. C 116 (2012) 18564–18570.
[25] J. Ota, S.K. Srivastava, J. Phys. Chem. C 111 (2007) 12260–12264.
[26] Y. Yu, C.H. Jin, R.H. Wang, Q. Chen, L.M. Peng, J. Phys. Chem. B 109 (2005) 18772–18776.
[27] Z.P. Liu, S. Peng, Q. Xie, Z.K. Hu, Y. Yang, S.Y. Zhang, Y.T. Qian, Adv. Mater. 15 (2003) 936–940.
[28] F. Abraham, B. Arab-Chapelet, M. Rivenet, C. Tamain, S. Grandjean, Coordin. Chem. Rev. 266–267 (2014) 28–68.
[29] H.B. Wu, H.H. Hng, X.W. Lou, Adv. Mater. 24 (2012) 2567–2571.
[30] H.Q. Chen, J.C. Ren, Talanta 99 (2012) 404–408.
[31] Y. Wang, M.Z. Huang, X.Y. Guan, Z.Q. Cao, F. Chen, X.P. Wang, Opt. Express 21 (2013) 31130–31137.
[32] H.F. Bao, X.Q. Cui, C.M. Li, Y. Gan, J. Zhang, J. Guo, J. Phys. Chem. C 111 (2007) 12279–12283.
[33] X.Y. Ma, L. Liu, W.L. Mo, H.J. Liu, H.Z. Kou, Y.Q. Wang, J. Cryst. Growth 306 (2007) 159–165.
[34] G.J. Xing, Z.J. Feng, G.H. Chen, W. Yao, X.M. Song, Mater. Lett. 57 (2003) 4555–4559.
[35] L.S. Li, N.J. Sun, Y.Y. Huang, Y. Qin, N.N. Zhao, J.N. Gao, M.X. Li, H.H. Zhou, L.M. Qi, Adv. Funct. Mater. 18 (2008) 1194–1201.
[36] B. Cheng, E.T. Samulski, Chem. Commun. 16 (2003) 2024–2025.
[37] J.M. Ma, J.Q. Yang, L.F. Jiao, T.H. Wang, J.B. Lian, X.C. Duan, W.J. Zheng, Dalton Trans. 40 (2011) 10100–10109.
[38] C.N.R. Rao, A. Govindaraj, Synthesis of inorganic nanotubes, in: K.E. Geckeler, H. Nishide (Eds.), Advanced Nanomaterials, Wiley-VCH Verlag GmbH & Co., KGaA, Weinheim, 2010, pp. 195–241.
[39] G.Q. Zhu, P. Liu, Cryst. Res. Technol. 44 (2009) 713–720.
[40] X.C. Jiang, Y. Xie, J. Lu, L.Y. Zhu, W. He, Y.T. Qian, Adv. Mater. 13 (2001) 1278–1281.
[41] Y.P. Li, F. Wei, Y.G. Ma, H. Zhang, Z.W. Gao, L. Dai, G.Q. Qin, CrystEngComm 15 (2013) 6611–6616.
[42] J.S. Chen, S.Y. Qin, G.X. Song, T.Y. Xiang, F. Xin, X.H. Yin, Dalton Trans. 42 (2013) 15133–15138.
[43] F.B. Li, X.Z. Li, Appl. Catal. A 228 (2002) 15–27.
[44] M. Salavati-Niasari, Z. Behfard, O. Amiri, E. Khosravifard, S.M. Hosseinpour-Mashkani, J. Clust. Sci. 24 (2013) 349–363.
[45] Z. Chen, N. Zhang, Y.J. Xu, CrystEngComm 15 (2013) 3022–3030.
[46] J. Zhang, S.Z. Qiao, L.F. Qi, J.G. Yu, Phys. Chem. Chem. Phys. 15 (2013) 12088–12094.
[47] F.X. Xiao, Chem. Commun. 48 (2012) 6538–6540.
[48] J. Wang, B. Li, J. Chen, N. Li, J. Zheng, J. Zhao, Z. Zhu, J. Alloys Comp. 535 (2012) 15–20.
[49] G. Yang, Q. Zhang, W. Chang, W. Yan, J. Alloys Comp. 580 (2013) 29–36.
[50] Y.R. Wang, W.L. Yang, L. Zhang, Y. Hu, X.W. Lou, Nanoscale 5 (2013) 10864–10867.
[51] S. Tuprakay, W. Liengcharernsit, J. Hazard. Mater. 124 (2005) 53–58.
[52] Y.C. Zhang, L. Yao, G. Zhang, D.D. Dionysioub, J. Li, X.H. Du, Appl. Catal. B – Environ. 144 (2014) 730–738.
[53] Q.P. Wu, J. Zhao, G.H. Qin, C.Y. Wang, X.L. Tong, S. Xue, Appl. Catal. B – Environ. 142–143 (2013) 142–148.
[54] S. Singh, B.R. Singh, W. Kha, A.H. Naqvi, J. Mol. Struct. 1056 (2014) 194–201.
[55] R.T. Hart, A.A. Kerr, N.A. Eckert, Tribol. Trans. 53 (2009) 22–28.